

# The Evolution of the South Atlantic Anomaly Measured by *RHESSI*

Bachelorarbeit

vorgelegt von  
Natalie Hell

Erlangen Centre for Astroparticle Physics  
Dr. Remeis-Sternwarte Bamberg  
Friedrich-Alexander-Universität  
Erlangen-Nürnberg

1. Gutachter: Prof. Dr. Jörn Wilms
2. Gutachter: Prof. Dr. Ulrich Heber

Tag der Abgabe: 02.08.2010



## Abstract

The South Atlantic Anomaly (SAA) is a region that contains an increased particle background due to a local minimum of the geomagnetic field. Because of this relation the trapped radiation follows the temporal variations of the Earth's magnetic field. The SAA's evolution in response to this variation together with other influences like the sun shall be determined. For this examination data taken with the Reuven Ramaty High Energy Solar Spectroscopic Imager (*RHESSI*) during early 2002 until the beginning of 2010 are used. The particle detector of this satellite has the advantage that it can distinguish between low energy particles, namely electrons, and higher energetic particles, i.e. protons. Being oppositely charged and due to the difference in their energy, both particles show slightly different behavior. Therefore, the analysis is applied separately for electrons and protons allowing for comparison of the results. Maps of the SAA are provided on a quarter of a year basis with a resolution of 10 km altitude and  $0.5^\circ$  in latitude and longitude. Furthermore, cuts at two different latitudes,  $-23^\circ$  for comparison with the Rossi X-ray Timing Explorer (*RXTE*) and  $-31^\circ$  through the center of the SAA, are made. It is shown that towards the center of the SAA a Gumbel distribution describes the particle flux sufficiently well whereas farther towards the northern edge of the SAA a Weibull distribution is a better choice. The norm of the fitting functions is used as a measure for the strength of the SAA whereas the maximum position of the same function accounts for the SAA maximum position. This position is found to be drifting westwards by about  $0.6^\circ \text{ yr}^{-1}$ . Additionally, the anti-correlation of the SAA strength to the solar activity is confirmed while at the same time the disturbance of the particle environment through large solar storms is shown.



# Contents

<b>1</b>	<b>Introduction</b>	<b>5</b>
1.1	Trapped Charged Particles . . . . .	6
1.2	Former Investigations . . . . .	10
1.3	The Reuven Ramaty High Energy Solar Spectroscopic Imager ( <i>RHESSI</i> ) . . . . .	12
1.3.1	Spacecraft Configuration . . . . .	12
1.3.2	Localization . . . . .	13
<b>2</b>	<b>The SAA Measured by <i>RHESSI</i></b>	<b>15</b>
2.1	Mapping the SAA . . . . .	15
2.2	The Shapes of the SAA . . . . .	17
2.3	Temporal Evolution of the SAA . . . . .	21
2.4	Position of the SAA Maximum . . . . .	23
<b>3</b>	<b>Outlook</b>	<b>28</b>
	<b>Bibliography</b>	<b>29</b>



# Chapter 1

## Introduction

In January 31, 1958, Explorer 1, the first U.S. satellite, was launched from Cape Canaveral. On board it carried Dr. Van Allen's cosmic ray counters, a single Geiger-Mueller tube. The detector was designed to measure background cosmic rays. Because of the overhasty launch due to the race between the USA and the Soviet Union for pioneering space and shooting satellites into stable orbits, Explorer 1 carried no tape data recorder as there had not been enough time to modify it. Data was hence directly sent to Earth from the spacecraft and provided puzzling results. During passes through low altitudes of a few 100 km, the submitted measurements met the expected amount of cosmic rays. But being in the region of  $> 1500$  km over South America as few as zero counts per second were reported (Prölss, 2001). Lacking an explanation for the vanishing of the cosmic radiation, it first was considered to be a malfunction of the instruments. Later the Explorer 3 mission, featured with a recorder, revealed that the Geiger counter had been saturated due to the strong radiation caused by charged particles trapped in the Earth's magnetic field. The van Allen radiation belts were discovered. Consequently, the majority of instruments carried to space in the late 1950s and 60s had the purpose to measure energetic electrons and protons. Quantitative comparisons between those missions were difficult as their measurements differed by a factor of up to 10. Though the qualitative results cumulated in a general understanding of the near Earth radiation environment (Barth et al., 2003).

The trapped radiation is collocated in toroidal belts that envelope the Earth and can be divided into two parts, the inner and the outer radiation belt (see figure 1.1). A thorough understanding of the distribution of the particle background is very important. The increased radiation can cause failures in the electronics of spacecrafts, saturate sensitive detectors, produce biased results in measurements of cosmic sources and reduce the life time of satellites but is even more a serious threat to the health of astronauts.

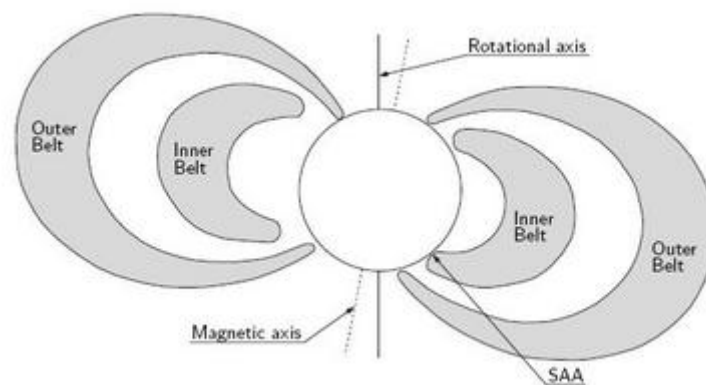


**Figure 1.1:** Sketch of the van Allen radiation belts (from [http://www.esa.int/TEC/Space\\_Environment/SEMEF3T4LZE\\_0.html](http://www.esa.int/TEC/Space_Environment/SEMEF3T4LZE_0.html)).

This work is about a special feature of the radiation environment: the South Atlantic Anomaly (SAA), a region of increased particle background above the South Atlantic Ocean, caused by a weakened Earth's magnetic field. Its movement and evolution as measured by the Reuven Ramaty High Energy Solar Spectroscopic Imager (*RHESSI*) is analyzed and compared to previous results. The findings of Fürst (2008) obtained from data taken by the Rossi X-ray Timing Explorer (*RXTE*) are of special interest as Fürst (2008) was the first to use a data set taken continuously with the same detector over a period of more than a decade. Moreover, measuring at similar energies, the life times of *RHESSI* and *RXTE* overlap from early 2002 up until now, their orbits passing through comparable altitudes. This overlap provides the unique possibility of a direct comparison between the results of both instruments. But *RHESSI* also has two advantages over *RXTE*. First, it has a greater inclination with respect to the equator. Thus, although it does not cover the SAA completely, in contrast to *RXTE* it cuts off only parts southern of the maximum. Additionally, the *RHESSI* particle detector is able to distinguish between low and high energy particles, namely electrons and protons. For the charge of electrons and protons having opposite sign, their response to the magnetic field is partially different.

## 1.1 Trapped Charged Particles

To understand what causes so many particles to crowd around the Earth, it is necessary to have a look at the Earth's magnetic field. The Earth's magnetism has already been well used e.g. for navigation, when William Gilbert published his book 'De Magnete' in 1600, where he claimed: 'Magnus magnes ipse est globus terrestris'. Even the westward drift of some features in the geomagnetic field has been known to 17th century navigators (Badhwar, 1997). In a crude approximation, the field's shape can be considered as a magnetic dipole which has an inclination of about  $11^\circ$  with respect to the Earth's rotational axis (Pinto et al., 1992). Additionally, the dipole has an offset of about 500 km from Earth's center towards Southeast Asia, which is increasing by  $2.5 \text{ km yr}^{-1}$  (Fraser-Smith, 1987). While this is just a model describing the experimentally determined shape, Elsasser (1946) proposed the nowadays most accepted theory for the physical formation of the field: the Dynamo Theory. Analyses of earthquake waves show that our planet's center is composed of a dense liquid core circulating around a solid inner core. It is believed that this liquid mainly consists of molten iron. These fluid motions, driven by convection and the Coriolis force, induce electric currents and hence magnetic fields. Moving a closed electric circuit through a magnetic field again results in induction. Thus these currents are self-reinforcing and stable, as shown by Roberts & Glatzmaier (2000) through magnetohydrodynamical calculations. Depending on turbulences and fluid dynamics of the molten iron, the emerging magnetic field is quite complex and underlies temporal variations. In fact, to characterize the shape of the field more exactly, other factors as magnetized rocks and the ring current in the magnetosphere have to be taken into account, too. But as this study focuses on trapped charged particles in near Earth regions, i.e. less than six Earth radii remote of the center, the dynamo approximation is sufficient enough. To keep track of the field's changes, the International Association of Geomagnetism and Aeronomy (IAGA) provides a new field model every five years, imaging the main field total intensity at the Earth's surface (see figure 1.2 on the next page). The plot is in good agreement with the eccentric dipole approximation. Both indicate the poles residing around  $130^\circ$  east and  $-60^\circ$  south and around  $100^\circ$  east and  $60^\circ$  north as well as the location of weakened field being around the South American continent and the south Atlantic ocean.

In the magnetic field charged particles can get caught, building a shell like structure as mentioned before. The mechanism of this capture and the movement of the trapped particles is complex, depending on inertia, friction and other external forces as well as the feedback of

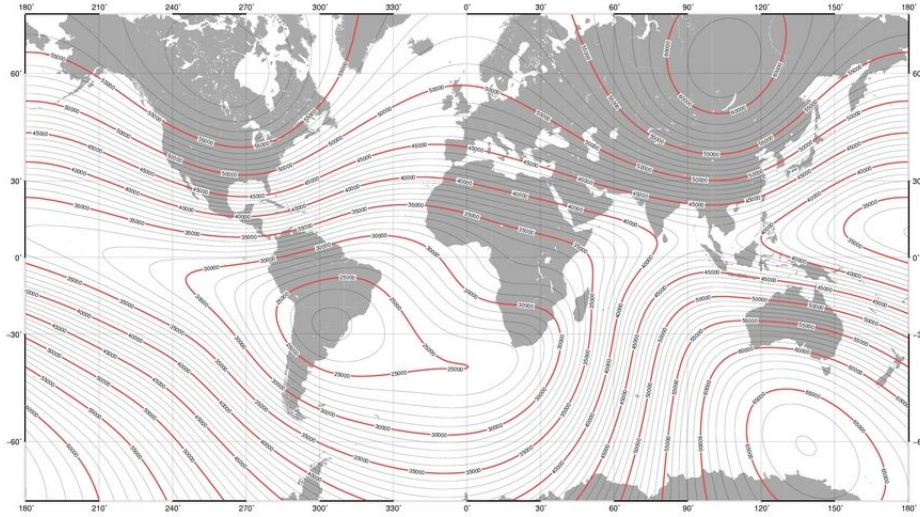


**Figure 1.2:** *Main Field Total Intensity of the 10th IGRF for the Epoch 2005 (from [ftp://ftp.ngdc.noaa.gov/Solid\\_Earth/Mainfld\\_Mag/images/F\\_map\\_mf\\_2005\\_large.jpeg](ftp://ftp.ngdc.noaa.gov/Solid_Earth/Mainfld_Mag/images/F_map_mf_2005_large.jpeg)).*

the particles movement to the field. Fortunately, many of those have such small effects on the particles and the field that they can be neglected. For example, because of the low density in the upper atmosphere, the cross section is small enough to neglect friction. Currents and their magnetic fields due to moved charges are diminutive and therefore almost not changing the Earth's magnetic field. So an easy model can be derived, starting with the Lorentz force  $\vec{F}_L = q(\vec{E} + \vec{v} \times \vec{B})$ . Anyhow, for the actual magnetic field this derivation can not be done analytically. Nevertheless using the dipole approximation gives a good insight into the processes of trapped radiation. The following calculations are based on Pröls (2001).

Because of the vector product  $\vec{v} \times \vec{B}$  only the particle's velocity component perpendicular to the magnetic field contributes to the Lorentz force. Thus, assuming a homogeneous magnetic field  $\vec{B}$  without any electric field, i.e.  $\vec{E} = 0$ , the Lorentz force simplifies to

$$F_L = qv_{\perp}B \quad (1.1)$$

where  $F_L$  points into the direction perpendicular to  $v_{\perp}$  and  $B$  and  $q$  is the absolute value of the charge. In equilibrium acceleration perpendicular to the velocity always results in a circular path. Via the balance of the Lorentz force with the centrifugal force the radius  $r_B$  of that circle can be determined.

$$F_{cen} = \frac{mv_{\perp}^2}{r_B} = qv_{\perp}B = F_L \quad (1.2)$$

and hence the so called Lamor- or gyroradius

$$r_B = \frac{mv_{\perp}}{qB}. \quad (1.3)$$

The direction of the gyration around the magnetic field line depends on the sign of the charge of the particle. For this reason, positive protons and negative electrons circle in opposite directions around the same guiding center. Remarkably, the gyration frequency  $\omega_B = v_{\perp}/r_B = \frac{qB}{m}$  is the same for all particles with same mass regardless of their energy and velocity. This is caused by the fact that higher energetic particles indeed fly faster but on that account are also forced onto a bigger circular path ( $r_B \sim v_{\perp}$ ). The so far neglected parallel component of the particle's velocity is unaffected by this configuration. Therefore both motions are superimposed linearly to form a helical path along the guiding magnetic field line. The declination between the path



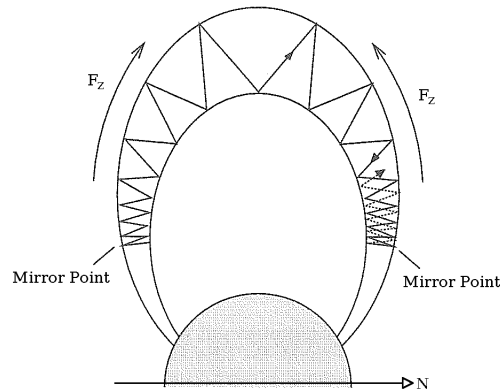


**Figure 1.4:** Sketch of the oscillation of a mirroring particle (after Prölss, 2001).

derived by a simple consideration. In a static magnetic field the energy of a particle is constant since the occurring forces are always perpendicular to the direction of motion. Accordingly, there must not be an accelerating electric field along the gyration path and therewith no electric potential. Faraday's law of induction links this potential with the temporal change of the magnetic flux  $\Phi$ . All in all from

$$U = -\frac{d\Phi}{dt} = -\frac{d}{dt}(r_B^2\pi B) = 0 \quad (1.7)$$

follows that during the oscillation the area surrounded by the gyration changes just enough for compensating the magnetic field gradient such that  $r_B^2\pi B = \text{const}$ . Inserting the gyro-radius (equation (1.3) on page 7) and the simple trigonometrical knowledge  $v_\perp = v \sin \alpha$ ,  $B/\sin^2 \alpha = \text{const}$  is obtained and therefore

$$B_{\text{mirror}} = \frac{B}{\sin^2 \alpha} = \frac{B_0}{\sin^2 \alpha_0} = \frac{B_{00}}{L^3 \sin^2 \alpha_0} \quad (1.8)$$

where  $B_0$  is the magnetic field strength at the apex and  $B_{00}$  is the same scaled after McIlwain's shell parameter  $L$ , which is the field line's distance to Earth's center in the magnetic equatorial plane measured in units of Earth radii (McIlwain, 1966). With this definition the field line proceeds along the path  $r = LR_E \cos^2 \lambda$ . Given that the field profile along a field line is known, the magnetic latitude  $\lambda$  and therefore the altitude of the mirror point can be calculated via

$$B_{\text{field line}} = \frac{B_{00}}{L^3} \frac{\sqrt{1 + 3 \sin^2 \lambda}}{\cos^6 \lambda} \quad (1.9)$$

which is derived from geometrical considerations of the magnetic field strength in spherical coordinates. In the case of the mirror point lying beneath the Earth's surface, the related particles get lost. The maximal angle  $\alpha_0$  for which this happens describes the so called loss cone. Only particles scattered into that cone can get released from their prison.

So particles with the same pitch angle always mirror at the same magnetic field strength. The South Atlantic Magnetic Anomaly (SAMA) is the location where the Earth's magnetic field is weakest. Therefore, the magnetic field intensity needed for mirroring is reached at lower altitudes, allowing the particles to immerge deeper into the atmosphere. As Lauriente et al. (1996) states, the peak of the particle distribution is a convolution of the properties of the particle ensemble and the magnetic field configuration. That means, there is no apriori requirement that the particle flux moves in unison with the magnetic field minimum. Nonetheless, charged particles are linked to the magnetic field, which leads to the SAA at least approximately following the westward drift of the SAMA. Therefore, the mirroring supplies a good explanation

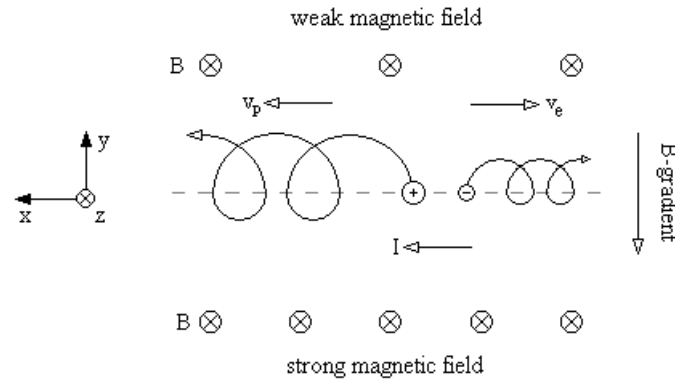


**Figure 1.5:** Sketch of the gradient drift in an inhomogeneous magnetic field with gradient perpendicular to field lines, producing a current  $I$  (after Prölss, 2001).

of the high radiation background in the SAA.

For a complete description of the influence of the magnetic field on the trapped particles, the B-field gradient perpendicular to the field strength is relevant, too. Although there are also other mechanisms, the two most important resulting effects are the gradient and the curvature drift. The gradient drift is based on the fact that the Larmor radius scales inverse with the magnetic field strength:  $r_B \sim B^{-1}$ . Therefore, in regions of weaker magnetic fields, the particles follow a circular path with larger radius. In reality a field gradient arises from the field strength of a dipole decreasing with increasing distance to the dipole axis and is rather continuous. Figure 1.5 shows a simplified picture where the gradient is approximated by a jump discontinuity. Here the particles travel along half circles that change their radii at the glitch between the two fields. In the higher field the covered distance is too small to reach the starting position again. That way with every turn the particle drifts away farther along the gyration plane. As the travel direction around the magnetic field line depends on the sign of the particle's charge, the net motion points in opposite directions for electrons and protons. Hence, a ring current around the Earth develops. The perpendicular gradient has its maximum at the equator, pointing towards Earth's surface. So positive particles drift westward whereas negative drift eastward.

The oscillation of the particles between the mirror points along the curved field lines create a centrifugal force. This force together with the B-field add up to an effective force parallel to the force causing the gradient drift. Therefore, the resulting curvature drift superimposes the gradient drift constructively generating an amplified overall drift.

Typical timescales for 20 MeV protons are 5 ms for the gyration period, 0.5 s for the oscillation period and 2 min for the drift period around the Earth. Since for these three movements the values of the timescales differ by several magnitudes, they can be linearly superimposed. Together they are responsible for the constitution of the shell like structure of the radiation belts. Due to the employed approximations, the mechanisms discussed above depict only the basic behavior and are subject to variations. For a more precise characterization of the particles' motions in the magnetosphere, additional effects have to be taken into account, e.g. collisions between the particles and the electric field present in the ionosphere.

## 1.2 Former Investigations

As a good knowledge of the particle background is important for protecting spacecrafts and especially for manned missions, many attempts have been made to determine the behavior of the South Atlantic Anomaly. There are three different methods to track its location proposed

by Heynderickx (1996) and discussed by Grigoryan et al. (2008): One can either monitor the motion of the eccentric dipole center, the local minimum of the geomagnetic field at fixed altitude in the SAMA region or the local particle flux maximum in the region of the SAA, as all three of these features originate from the same eccentric dipole approximation. Despite or actually because of this threefolded definition, it is not possible to determine the exact position of the SAA. Heirtzler (2002) argues that the position results obtained from these three methods may differ from each other by up to  $10^\circ$  latitude and  $20^\circ$  longitude. A reason for that is for example the energy dependence of the SAA position on the particle energy: the higher the energy, the better the flux maximum and the location of the geomagnetic minimum agree (Heynderickx, 1996; Grigoryan et al., 2005).

Before any standardized model was published, every scientist extrapolated and interpreted the existing data for his or her needs. The first model by Dr. Wilmot Hess at the NASA Goddard Space Flight Center has been too complicated to be effectively usable (Gaffey & Bilitza, 1990). Therefore, in 1976 it was followed by the work of Sawyer & Vette (1976) who released the AP-8 model for protons based on all data taken after 1970. A similar model for electrons (AE-8) was not put out until 1991 by Vette (1991). Together they include data measured by 43 satellites in 1630 channel-month (Barth et al., 2003). Both models are separated into two versions, AE-8/AP-8 MIN for solar minimum and AE-8/AP-8 MAX for solar maximum. While AE-8 shows at least a local time dependency, AP-8 is static and does not address any secular variations of the magnetic field except for the solar cycle. Nevertheless, until today these models are still the most commonly used. Garrett & Hastings (1994) advice caution since meanwhile the models are quite old and derived from data of less sophisticated instruments. Moreover, these models are biased inter alia by the continuously changing particle background, the individuality of each solar cycle and the neutron decay from atomic bomb tests in the atmosphere, which today are forbidden.

Konradi et al. (1994) and Badhwar et al. (1994) both use several shuttle flights in 1990/91 to find the maximum flux having moved by about  $0.32^\circ \text{ yr}^{-1}$  to the west during the last two decades compared to the AP-8 model. The same ansatz was made by Bühler et al. (1996) with data of *MIR* indicating a slope of  $0.26^\circ \text{ yr}^{-1}$ . To avoid relying on this model and to employ data taken by similar instruments, Badhwar (1997) compared measurements of *Skylab* in December 1973 and January 1974 to those of *MIR* of March 1995, leading to a drift rate of  $0.28^\circ \text{ yr}^{-1}$  westwards and  $0.08^\circ \text{ yr}^{-1}$  northwards during the 21.2 year period. The comparison of the Tri-Service Experiment Mission 5 (*TSX-5*, 2000-2006) with the Advanced Photovoltaic and Electronic Experiments (*APEX*, 1994-1996) by Ginet et al. (2007) yields a displacement of  $0.43 \pm 0.13^\circ \text{ yr}^{-1}$ . The relatively high uncertainty comes from the maximum position being averaged over the whole period of each of the two missions. Another approach was undertaken by Heirtzler (2002) and Heynderickx (1996) by determining the local minimum of the geomagnetic field via the International Geomagnetic Reference Field (IGRF). This effort induces a movement of roughly  $0.2^\circ$ . Adolphsen et al. (1995), Lauriente et al. (1996) and Mullen et al. (1998) followed a completely different path. They indirectly measured the particle flux by recorded Single Event Upsets (SEU) and Single Event Effects (SEE) respectively. These are instrumental malfunctions due to interactions with single particles and underly higher uncertainties as they can be caused by particles with different energies as well as by cosmic rays. Hence, the determined drift rate ranges between  $0.19^\circ \text{ yr}^{-1}$  and  $0.4^\circ \text{ yr}^{-1}$ .

Despite of the differences in the absolute position of the SAA investigated by the three models, the relative change of position is in very good agreement between them. Anyway, all of those investigations have the problem to depend on the comparison of data sets of different origin, either between different instruments on various missions under unequal conditions or between one mission and the overaged AP-8/AE-8 models. Grigoryan et al. (2005) has shown that the SAA features different sizes and locations at different energy bands. Therewith not only

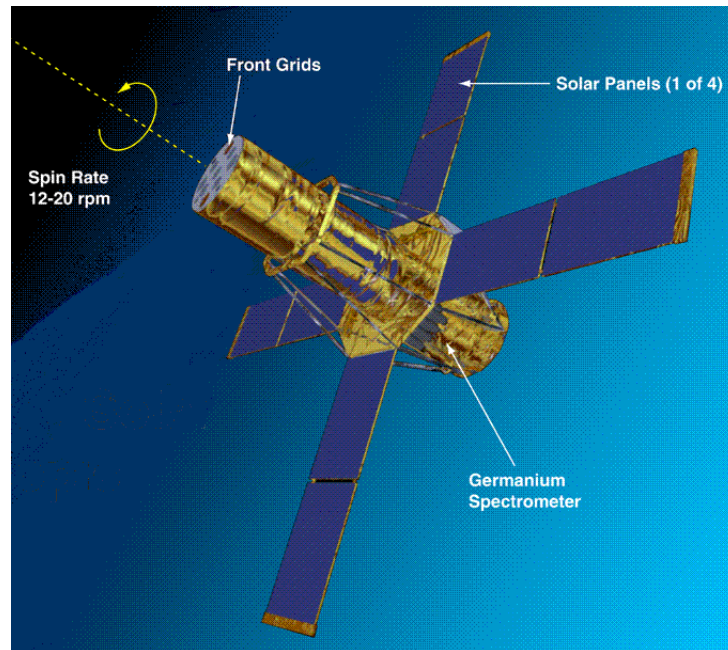


**Figure 1.6:** *Concept of RHESSI* (<http://hesperia.gsfc.nasa.gov/hessi/images/hessicraft.gif>).

mistakes in the results are put up but neither is it possible to spot short time variations in the drift rate. Fürst et al. (2009) analyzing the SAA as seen by the Rossi X-ray Timing Explorer (*RXTE*) have been the first to use a set of data continuously measured over a period of 12 years between 1996 and 2007, thus having seen a complete solar cycle. They designate an overall slope of  $0.290(2)^\circ \text{ yr}^{-1}$  but encounter two breaks in the drift rate in 1998 and 2003. It is suggested that those are connected to geomagnetic jerks that occurred at approximately the same time. An even longer time span from 1991 to 2009 is covered by the Along Track Scanning Radiometer (*ATSR*) (Casadio & Arino ,priv. comm.). Here the radiation background is reconstructed via hot spots in the instrument. Their calculated drift rate of  $0.35^\circ \text{ yr}^{-1}$  westward and  $0.12^\circ \text{ yr}^{-1}$  northward is in good agreement with former results. Additionally, they claim to confirm the influence of the jerk of 2003 and add another one at 1991.

## 1.3 The Reuven Ramaty High Energy Solar Spectroscopic Imager (*RHESSI*)

### 1.3.1 Spacecraft Configuration

On February 5th 2002 the High Energy Solar Spectroscopic Imager (*HESSI*) was launched by a Pegasus XL Rocket as one of NASA's Small Explorer missions. Although planned as a mission with a life time of two years and a possible extend to three years, *HESSI* has already provided data for 9.5 years. Initially, it was shot into a circular low earth orbit with an inclination of  $38^\circ$  at 600 km altitude which meanwhile has stabilized at  $\sim 560$  km. The primary objective of this mission is to monitor X-rays and gamma rays from solar flares and to investigate the fundamental processes of particle acceleration and explosive energy release (Hajdas et al., 2004). Following its launch, it was renamed *RHESSI* to honor the deceased Reuven Ramaty who was a pioneer in solar flare research and a great supporter of the mission.

With a total weight of 300 kg and a scientific payload of 120 kg, *RHESSI* consists mainly of nine segmented, hyperpure germanium crystal spectrometers cooled to approximately 75 K. To

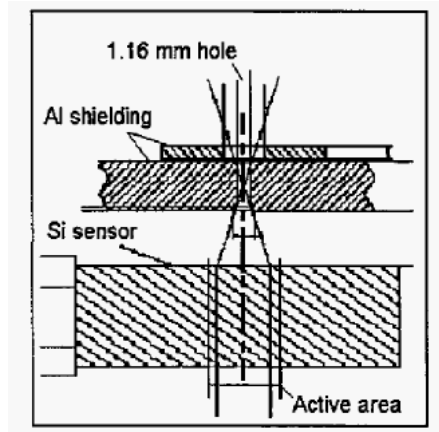


**Figure 1.7:** Sketch of the RHESSI particle detector (Hajdas et al., 2004).

save weight for the scientific instrumentation, *RHESSI* is not heavily shielded and hence is a high background detector. Nevertheless, the spacecraft is additionally equipped with a standard silicium charged particle detector for health purposes and in order to guarantee good quality of the data obtained by the Ge-detectors. During periods of high energy radiation events, e.g. SAA transits, no data is taken by the spectrometer but only by the particle detectors.

The particle detector measures 0.564 cm in diameter and is 1 mm thick. It has a 1.7 cm Aluminium cylinder as side shielding. The 3.8 mm thick Aluminium front window with 3.86 cm diameter has a small opening of 1.16 mm diameter that is covered by 2.54  $\mu\text{m}$  thick Nickel foil. There are two energy thresholds for deposition of incoming particles. The lower at 50 keV is fixed whereas the second at 650 keV is commandable in the range of 20 keV up to 2 MeV. The data were taken using the same threshold over the whole period of the mission, though. With this configuration electrons above 70 keV at a small solid angle are detected in the lower and protons above 28 MeV through a larger solid angle in the upper threshold. Due to the specific energy loss of high energy electrons in the thin Si-detector, the detection efficiency for electrons in the upper threshold is small; however, because of the electrons being more numerous than the protons, the detection rate of the upper energy channel is still slightly contaminated by electrons. Additionally, outside the SAA the particle detector mainly measures the cosmic ray flux as cosmic rays can penetrate the shielding easily and usually trigger both thresholds. Since the detector's distinguishing of particles works so well, the detected low energy particles are in the following referred to as electrons whereas the high energy particles will be called protons.

The detector is mounted facing outwards on a strut running past the side of the spectrometer. Its normal axis is perpendicular to the spacecraft axis. *RHESSI* itself points almost always into the direction of the sun, rotating with a period of 4 sec. Therefore, having a readout every eighth of a second it provides the possibility to detect particle flux anisotropies. Especially, whenever the rotation axis is nearly perpendicular to the local magnetic field lines, *RHESSI* sees the pitch-angle distribution of particles being extremely flat and pancake like. This actually meets the expectation as mirroring particles circle at pitch angles of almost  $90^\circ$  with respect to the field lines (Smith et al., 2002).

### 1.3.2 Localization

The position of *RHESSI* in latitude, longitude and altitude is calculated via two different algorithms working differently well and stable. Usually, the results of these two differ by roughly 0.5 km in altitude but almost never in latitude and longitude. With few exceptions both algorithms provide smooth orbits with no major jumps in positions. But the first algorithm

has three faults. Sometimes no numerical value is given at all. On other occasions, the derived altitude is suggested to be constant equal to  $-6378.13$  km for a while. Being obviously wrong, these two miscalculations can easily be filtered out. The third defect is much more delicate. According to the algorithm, the satellite seems to jump occasionally from its orbit at 540 km to 600 km altitude to less than 500 km and back again within short time, which is a rather unrealistic behavior for a spacecraft. In contrast, the second algorithm produces no such outliers except for three months in 2006. From March to May the position calculation via the second algorithm completely failed, claiming an altitude of minus earth radius. To compensate for the missing position information, in March and May all positions where the calculated altitude of the first algorithm is smaller than 500 km are linearly interpolated between the last and the next believable entry. However, in April the sequence of corrupted positions is too long for this procedure. Therefore, throughout the whole analysis the second algorithm is used with one substitution in 2006 and April of the same year is omitted completely.

For further information about *RHESSI* and its mission see Hajdas et al. (2004), Smith et al. (2002) and <http://hesperia.gsfc.nasa.gov>.

# Chapter 2

## The SAA Measured by *RHESSI*

### 2.1 Mapping the SAA

As a *RHESSI* orbit covers only a small region of the sky, the data has to be reorganized and collected over certain time and altitude intervals in order to see the shape and location of the SAA. Although the particle flux is read out every 0.125 s (Smith et al., 2002), the measurements are combined to one data point per 4 s. This corresponds to an average over about one spin of the satellite. Since *RHESSI*'s position information has only a resolution of 60 s, the actual positions are linearly interpolated according to the time-stamps of the monitor files. Then they are rebinned into  $0.5^\circ$  in latitude and  $0.5^\circ$  in longitude and projected onto a world map for better orientation. Each map represents the data taken in a 10 km altitude interval during a period of three months. Table 2.1 lists the existing altitude time combinations and allocates them with the color code used in later plots. *RHESSI*'s ability to distinguish between electrons and protons is respected by mapping them separately.

The choice of these intervals is a compromise mainly between two objectives: to obtain high spatial and temporal resolution with a good signal to noise ratio as well as to create maps comparable to those of Fürst et al. (2009) who binned their data into  $0.25^\circ$  in longitude but in the same latitude, altitude and time periods. So *RXTE*'s resolution is twice as good as it is possible for *RHESSI*. This is due to the missions' different applicabilities for the analysis of the SAA maximum. Projected onto the Earth's surface the satellite orbits are sinusoidal. Thus, towards the edges of the covered area the satellites remain longer in the same latitudes, resulting in an increased number of measurements per bin. As the maximum of the SAA lies outside of the stripe covered by *RXTE*, the analysis was done using the southernmost latitudes, i.e. the latitudes with the highest number of measurements per bin. There, a small number of measurements near the equatorial regions is acceptable. In contrast, *RHESSI* cuts off only parts south of the SAA maximum. Therefore, also latitudes smaller than the inclination have to provide good statistics in order to fit the maximum position at  $-23^\circ$  south for comparison

**Table 2.1:** Colors used to depict altitudes in the plots. The last column lists the time bins in which the data is available. Each time bin is 3 months in duration, named after the lower limit of the interval.

Color	Altitudes ( km)	Time Bins
red	590 – 599	2002.0 – 2003.0
magenta	580 – 589	2002.0 – 2005.0
orange	570 – 579	2002.0 – 2010.0
green	560 – 569	2002.75 – 2010.0
blue	550 – 559	2004.0 – 2010.0

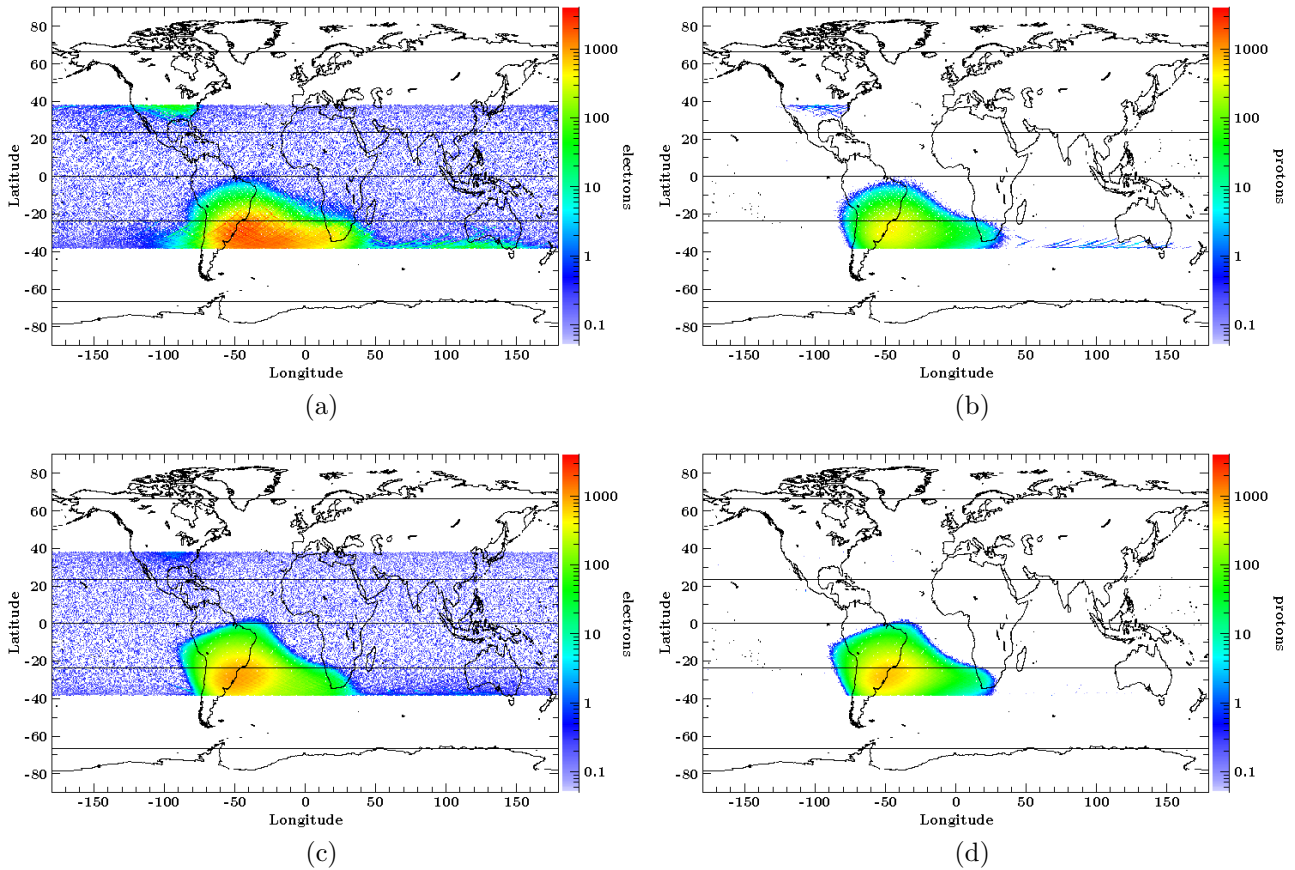


**Figure 2.1:** Maps of the particle background for (a) electrons and (b) protons at altitude 570 km – 579 km in 2002, 4th quarter, and (c) electrons and (d) protons at altitude 560 km – 569 km in 2009, 2nd quarter.

with the results of Fürst et al. (2009) and the actual maximum at about  $-31^\circ$  south. With the chosen resolution *RHESSI* passes through each latitude-longitude-altitude bin 4.4 times on average per quarter of the year.

Figure 2.1 shows examples for the generated maps. The lines indicating the region of the tropics coincide with the maximum latitude reached by *RXTE* and thus provide an easy comparison between the two satellites. Electrons (left) and protons (right) are displayed near the beginning of the mission (top) and the end of the used data set (bottom) to demonstrate the change of the SAA over the years. Obviously, the electron flux tends to be higher than the proton flux. Additionally, Badavi et al. (2005) result is confirmed who claim that almost all of the trapped proton flux in low Earth orbit is located in the SAA. Besides the SAA there are two other features visible in the maps. Above North America resides a smaller counterpart of the SAA (see figure 1.2 on page 7) of which the southern edge reaches into *RHESSI*'s field of view. The third region of increased background radiation is the north-eastern edge of the southern polar horn. Polar horns are a region where at high latitudes the outer radiation belt comes close to Earth.

Since there are differences in the particle distributions of electrons and protons, depicting the ratio between the two of them may lead to additional perceptions. Due to the different energies of electrons and protons, the ratio of their number describes just as well the energy distribution. Figure 2.2 on the facing page shows that there are distinctly more electrons than protons at the eastern boundary of the SAA whereas their number gets more similar to each other towards the west. The orientation of the stripes with respect to the coordinate axes and the apparent minimum of the particle ratio approximately at the position of the SAA maximum

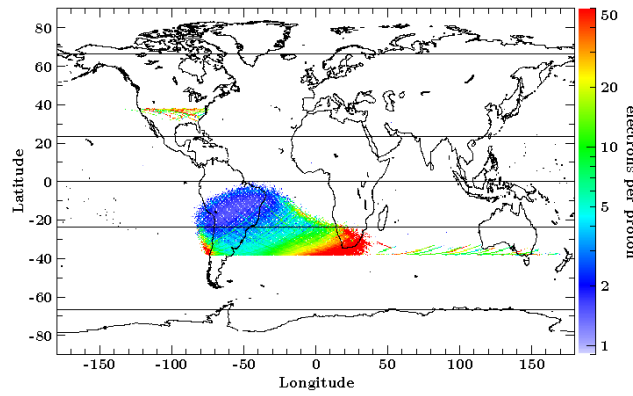


**Figure 2.2:** Map of the electron per proton ratio at altitude 570 km – 579 km in 2002, 4th quarter.

remind of the region of magnetic minimum visible in the contour plots of the intensity of the geomagnetic main field (figure 1.2 on page 7). In fact, the altitude of the mirror points of a particle depend on its pitch angle which again is a function of the particle velocity and, with it, the particle energy. Accordingly, higher energetic particles, i.e. protons, dominate in the northwest around the center of the SAA, where at the same altitudes the magnetic field is weaker than in the southeast. Therefore, the electron-proton-ratio varies over the SAA since different energy spectra are measured.

## 2.2 The Shapes of the SAA

As mention before, the *RHESSI* results shall be compared with those of Fürst et al. (2009) using *RXTE* data. The most direct way to do so is to look at the shape of the SAA at the same latitude, i.e.  $-23^\circ$ . Many former attempts to fit the shape take a Gaussian distribution as basis (see, e.g., Badhwar et al., 1994; Konradi et al., 1994; Bühler et al., 1996). But as can be seen in figure 2.3 on the following page and even in figure 2.1 on the preceding page the shape of the SAA is rather asymmetric with a tail towards longitudes east. For this reason, Fürst et al. (2009) have shown that the Weibull function delivers a significantly better description. Originally intended to describe the life time of light bulbs (Barlow, 1989), the Weibull distribution has the form

$$W(x) = \begin{cases} A_w \cdot \frac{k}{\lambda} \cdot \left(\frac{x-\theta}{\lambda}\right)^{k-1} \cdot \exp\left(-\left(\frac{x-\theta}{\lambda}\right)^k\right) & \text{for } x > \theta \\ 0 & \text{else} \end{cases} \quad (2.1)$$

where  $A$  is the normalization parameter,  $\lambda$  the scale parameter,  $k$  the shape parameter and  $\theta$  the shift parameter. Mean  $\mu_W$  and variance  $\sigma_W^2$  are given by

$$\mu_W = \lambda \cdot \Gamma\left(\frac{1}{k} + 1\right) + \theta \quad (2.2)$$

$$\sigma_W^2 = \lambda^2 \cdot \left(\Gamma\left(\frac{2}{k} + 1\right) - \Gamma\left(\frac{1}{k} + 1\right)^2\right) \quad (2.3)$$

with Euler's Gamma function  $\Gamma(z) = \int_0^\infty t^{z-1} e^{-t} dt$ . As the movement of the SAA maximum is one of the aspects under examination, the maximum position of the Weibull function is of interest. It can be calculated via

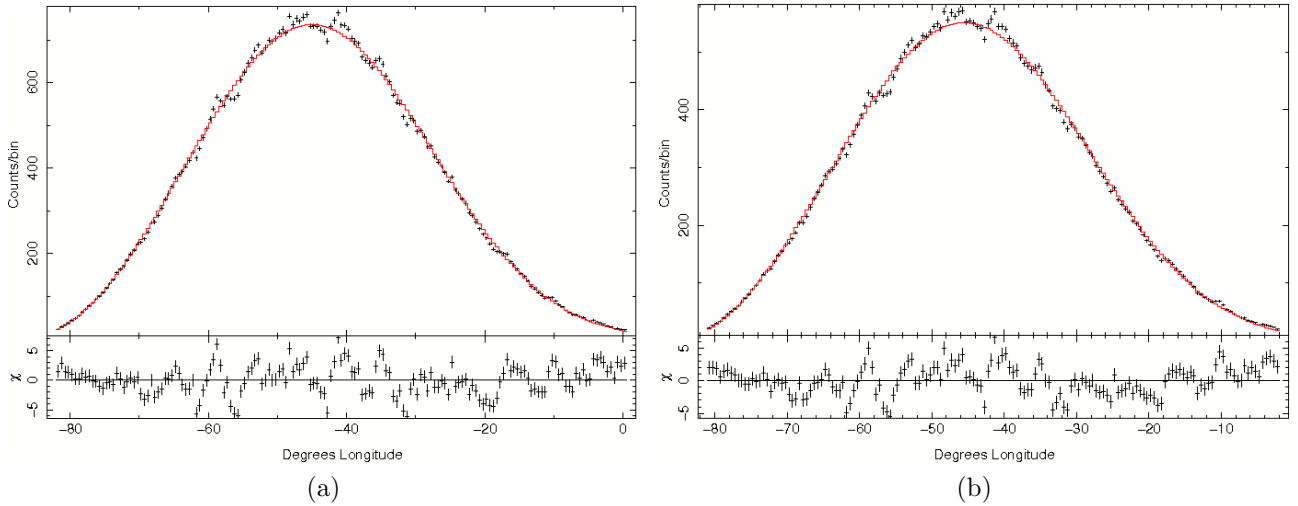


**Figure 2.3:** Weibull fit of (a) electrons and (b) protons for latitude  $-23^\circ$  south, altitude 560 km – 569 km in 2009, 2nd quarter.

$$x_{\max} = \lambda \cdot \left( \frac{k-1}{k} \right)^{\frac{1}{k}} + \theta \quad (2.4)$$

According to Grigoryan et al. (2005), although there are SAA features that change with altitude, the change in the location is independent of it. This is also seen by Fürst et al. (2009) and confirmed by the following results at least during the time intervals with good statistics. However, obviously the shape of the SAA is a function of latitude (see figure 2.1 on page 16). The Weibull distribution is not able to compensate at the same time for increasing particle flux and extending of the tail farther towards east with increasing latitudes south. So for the same analysis approach near the SAA maximum at latitude  $-31^\circ$  a new fitting function is needed. Numerical testing of various distributions revealed that actually the log-Weibull distribution

$$G(x) = A_g \cdot \frac{1}{\beta} \cdot \exp \left( -\frac{x-\alpha}{\beta} - \exp \left( -\frac{x-\alpha}{\beta} \right) \right) \quad (2.5)$$

called Gumbel distribution is a sufficiently good description of the particle flux (see figure 2.4 on the next page). Here,  $A_g$  again is the normalization parameter,  $\beta$  the scale parameter and  $\alpha$  is the mode of the distribution, i.e.  $x_{\max} = \alpha$ . Then mean  $\mu_G$  and variance  $\sigma_G^2$  can be written as

$$\mu_G = \alpha + \gamma\beta \quad (2.6)$$

$$\sigma_G^2 = \frac{(\beta\pi)^2}{6} \quad (2.7)$$

where  $\gamma = 0.57772\dots$  is the Euler constant (Antal et al., 2009). Overall, the Weibull and the Gumbel distributions represent the basic distribution of the radiation background. Yet, there are overlaid structures to be dealt with. Therefore, in both cases the fits are done using an average over a total of  $2^\circ$  in latitude to increase the considered number of count rates per bin for better statistics. The change between the latitude averaged over is negligible so that the resolution of the relevant parameters is not reduced.

The temporal variation of the strength and the general change of the maximum position of the SAA are both specified by the continuum of the distribution. Therefore, the main interest lies in fitting the continuum. Added to this continuum is a seemingly periodic structure that is more regular than ordinary noise and needs to be understood, too. This pattern occurs

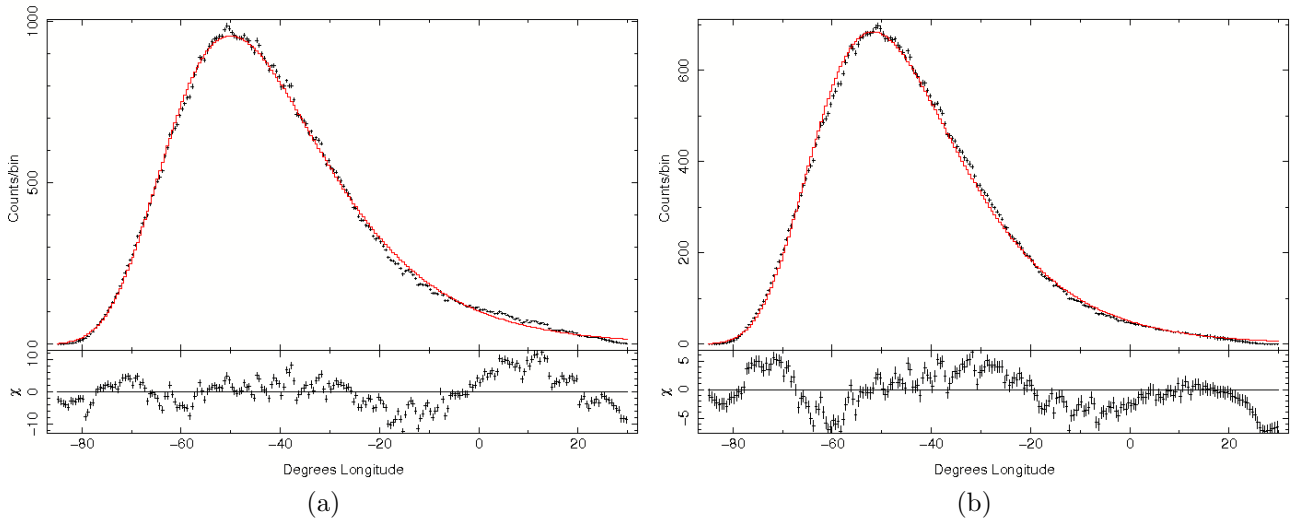


**Figure 2.4:** Gumbel fit of (a) electrons and (b) protons for latitude  $-31^\circ$  south, altitude 560 km – 569 km in 2009, 2nd quarter.

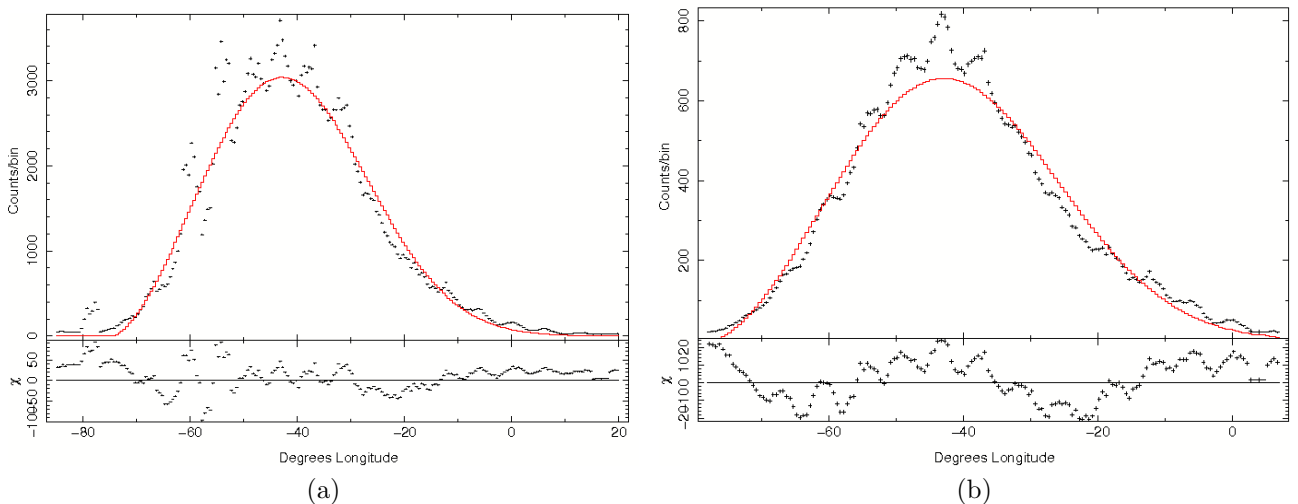


**Figure 2.5:** Example of noise for (a) electrons and (b) protons for latitude  $-23^\circ$  south, altitude 570 km – 579 km in 2005, 1st quarter.

equally for electrons and protons as well in the Weibull fits as in the Gumbel fits and is most in the years 2003 to 2006. During this time the quality of the fits (figure 2.6 on the following page) is reduced dramatically not only because their fundamental form can not account for the additional structure but also because the actual continuum is missed due to the trial to include this structure. Thus, the exact maximum position determination is affected as will be an issue later on.

To exclude an impact through solar flares which should mostly be visible during the day time of the satellite, the *RHESSI* data are separated for day and night. This is done by calculating the azimuth of the sun at the location of the spacecraft. As *RHESSI* is located few hundred kilometers above the ground, due to the transparency of the atmosphere the sun has to be farther under the horizon than a certain angle, which can be derived from simple geometry, in order to be covered by the Earth from *RHESSI*'s point of view. This effort did not solve the problem but rather increased the effect since it separated measurements that had averaged each other out beforehand.

Another attempt to smooth the distribution in each latitude is to solely apply the analysis to

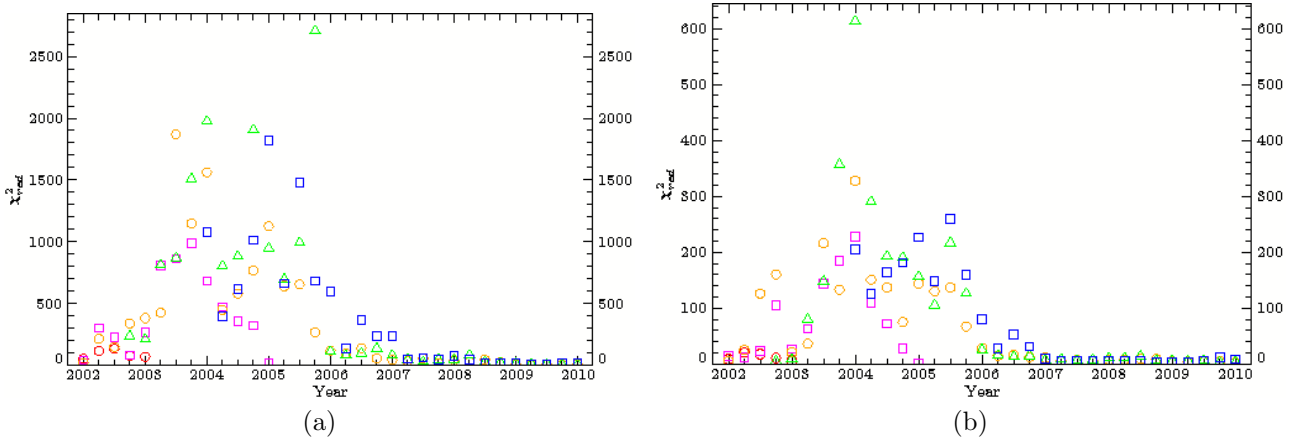


**Figure 2.6:** Reduced  $\chi^2$  of the Weibull fits at latitude  $-23^\circ$  south for (a) electrons and (b) protons.

the median of each bin. Resolving the individual entries per bin reveals that the count rates of measurements separated only by a few seconds are of the same order of magnitudes whereas those separated by longer timescales may differ by several magnitudes. This effect was also observed by Pinto et al. (1992). With the number of measurements taken at approximately the same position, i.e. the same latitude, longitude and altitude within a few seconds, depending on the orbit's angle and intersection of a latitude-longitude-bin, the median of such a collection emerges as a quite random variable as the total amount of data points per bin is still very small. Hence, the unwanted substructure is reproduced. For the same reasons filtering the data via quantiles, in this manner neglecting the highest and lowest ten percent of the measurements within each data bin, is not successful.

Since the structure is spatially resolved rather than noise randomly distributed around the basic function, these approaches may not provide the right solution. Additionally, the width in longitude of the peaks is greater than the sum of longitude bins that would be passed in a row by a single orbit at the examined latitudes plus it takes some time for two orbits to reach similar longitudes at the same latitude. Thus, it is unlikely that they are caused by single solar flares. A possible explanation might be presented by the instruments which took the employed data. Though apparently there are no jumps in the orbits obtained from the positioning files, any malfunctioning of the algorithm and effects of the instruments can not be completely excluded. For example, in the quarter of 2005.75 the calculated orbits show strange behavior. Having the same amount of data as all the other quarters, the coverage of the sky is far worse. Looking into the orbit plot (figure 2.7b on the next page) it can be seen that a few orbits are reproduced again and again. This is unusual compared to other quarters where the interstice between two consecutive orbits is filled almost entirely over the three month time by the shift of the orbit that is caused because after one period in latitude the period in longitude is not yet completed. Moreover, those shifts appear in longitudinal direction only such that the orbits are pairwise parallel when projected onto the Earth's surface. But in this specific quarter there obviously are some that went astray.

However, it is conspicuous that after the big deficiency in 2006 mentioned in section 1.3.2 on page 13 the data and statistics get significantly better. Nevertheless, the emission lines do not vanish completely but get far less intense, disturbing the fits far less. Another explanation could be that around the same time the particle flux (see, e.g., figure 2.8 on page 22) is again reduced to about the level of the beginning of the mission while at the same time being more consistent between the different altitudes.

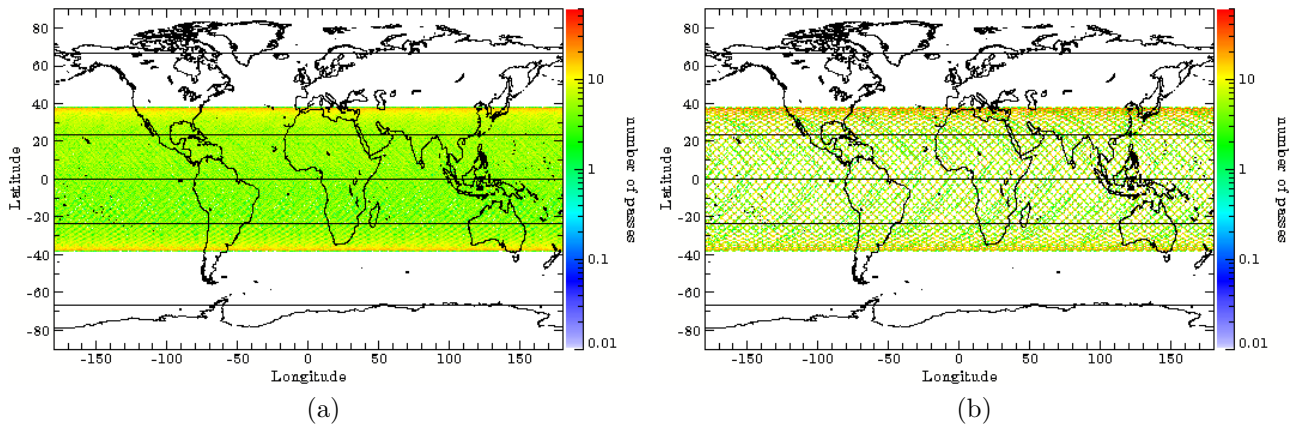


**Figure 2.7:** Orbits of RHESSI for (a) 560 km – 569 km in 2009, 2nd quarter, compared to (b) orbits in 4th quarter of 2005, altitude 560 km – 569 km.

## 2.3 Temporal Evolution of the SAA

There are several ways to determine the strength of the SAA. Either properties of the fitting function, such as the normalization factor, the maximum value and the integral, can be used as a measure for the strength or, independent of the quality of the fit, just the sum over all count rate entries falling into a predefined area around the SAA. Huston et al. (1996) and Dachev et al. (1999) have demonstrated that the strength of the SAA is anti-correlated to the solar activity. During the maximum of the solar cycle the upper atmosphere gets heated, which leads to an increased neutral density in the lower parts of the atmosphere where the satellite resides. This is followed by a higher absorption of trapped particles with the consequence that fewer particles mirror at the altitude of the satellite. Thus, the measured particle flux is reduced compared to times of solar minimum.

To calculate the sum over a certain region has already been done by Bühler et al. (1996). They took into account all data points within a rectangle defined by  $-80^\circ \leq \text{longitude} \leq 40^\circ$  and all latitudes south of the geographic equator. The summed up count rate in each quartal is averaged over the number of considered data points to avoid differences due to differences in the number of measurements and unequally thorough covering of the region. The result is illustrated in figure 2.8 on the following page, again separated for electrons and protons. For comparison with the solar activity, the solar 10.7 cm radio flux is plotted on the second  $y$ -axis. The data of the radio flux is provided by the National Geophysics Data Center (NGDC)<sup>1</sup>. Here, the monthly average is taken.

As the norm, the integral of the fitting function and the functions maximum value all depend on the same fit parameters, these graphs show no big differences. Thus, here only the normalization of the fits is displayed. See figure 2.9 on the next page for the results of the Weibull fits at latitude  $-23^\circ$  and figure 2.10 on the following page for those of the Gumbel fits at  $-31^\circ$ .

In contrast to the predicted anti-correlation, there obviously is a great peak visible around 2003 after the solar maximum but still before the solar minimum. Since it arises equally in both, the fitted and the summed up count rates, an effect of the low fit quality during the time in question can be excluded, implying that this excess in count rate actually is in the data and indicates the physical behavior of the SAA. According to Baker et al. (2004) during the last quarter of the year 2003 a great number of exceptional heavy solar storms occurred. As a consequence, the outer radiation belt was extremely distorted and displaced inwards towards the Earth. Because of this, the slot region, i.e. the region between the inner and the outer

<sup>1</sup><http://www.ngdc.noaa.gov/>

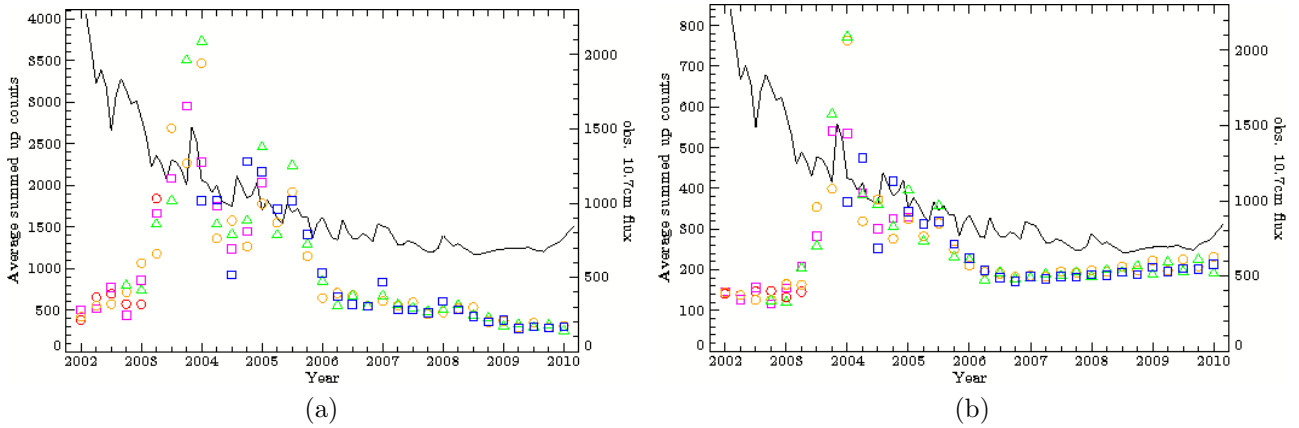


**Figure 2.8:** Averaged summed up count rates in the region between longitudes  $-80^\circ$  and  $40^\circ$  and latitudes  $\leq 0^\circ$  vs solar radio flux (black line): (a) electrons and (b) protons.

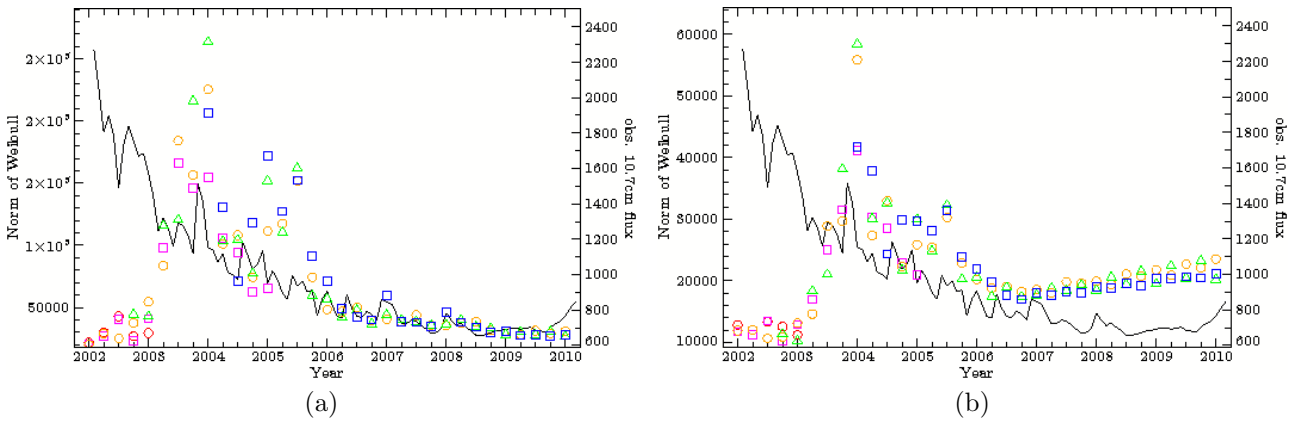


**Figure 2.9:** Norm of Weibull at latitude  $-23^\circ$  south vs solar radio flux: (a) electrons and (b) protons.

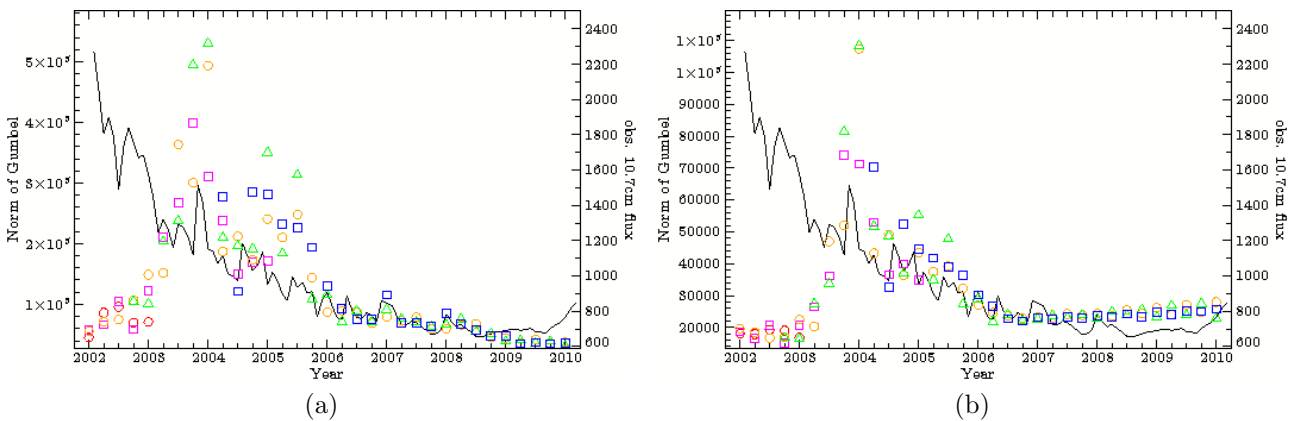


**Figure 2.10:** Norm of Gumbel at latitude  $-31^\circ$  south vs solar radio flux: (a) electrons and (b) protons.

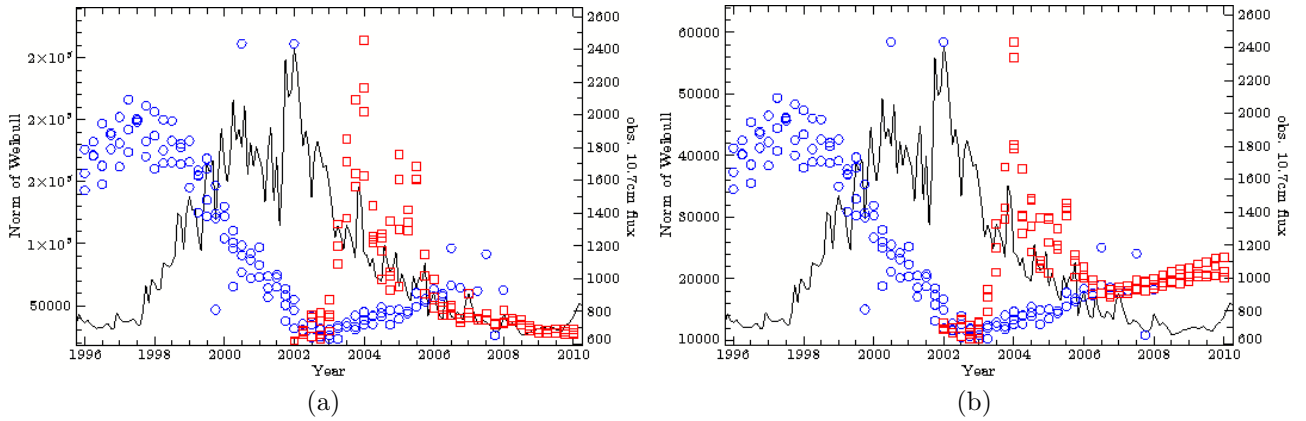


**Figure 2.11:** Norm of Weibull at latitude  $-23^\circ$  south of *RHESSI* (red) and *RXTE* (blue, rescaled to the values of *RHESSI*) vs solar radio flux (black): (a) electrons and (b) protons.

belts where particles are normally not able to survive on any longer time scales, was filled with particles and held even higher amounts of radiation than the region of the usual outer belt. Accordingly, at the same time a huge population of energetic particles was injected into the inner belt, so to say at the location of *RHESSI*. The consequences of this event are said to have been very long lasting as is also reflected in figures 2.8, 2.9 and 2.10. This out of order increase is also seen by *RXTE* but in a far lesser extent (see norm of Weibull plot in figure 2.3.10 of Fürst, 2008). A reason for that might be that the threshold energy of *RXTE*'s particle monitor is about 500 keV for electrons whereas the *RHESSI* particle monitor is able to detect electrons at an energy of 70 keV already. The additional low energy electrons may lead to that discrepancy as the particle energy of solar wind electrons typically lies in the range of few 10 keV up to a few 100 keV (Li et al., 1997).

Since this outburst dominates a wide time range of the total examined period, the aforementioned anti-correlation between the particle flux and the solar activity is not directly obvious. For the protons the particle flux is increasing slowly but the electron flux seems to stay rather constant. Nevertheless, a comparison between the norm of the Weibull fit of data taken by *RXTE* and *RHESSI* confirms the inverse correlation of the particle flux to the solar activity (see figure 2.11). Hereby an effect already stated by Huston et al. (1996) can be seen. They studied the particle flux over the period of almost two solar cycles and at several L-values and found that the rate of decrease in the proton flux during the rising part of the solar cycle is much faster than the increase during decreasing solar activity. Moreover, each particle flux minimum shows its own characteristic behavior: sometimes the particle flux goes up immediately after reaching the minimum while it remains there for a while at other times. This also is in agreement with Casadio & Arino (priv. comm.) who analyzed a continuous data set ranging from 1991 up to now finding that although following the expectations the SAA count rates tend to stay lower in the approaching solar minimum than in the previous one.

## 2.4 Position of the SAA Maximum

Finally, the temporal movement of the maximum of the SAA is determined using the longitude of the maximum value of the Weibull and Gumbel fits as a measure. These are displayed in figure 2.12 on page 25 separately for electron and protons, each for the two different examined latitudes. Generally, the overall trend is the same in all four of them and in the *RXTE* results. The absolute value in longitude on the contrary differs by a few degrees between the different

latitudes and satellites. The reason for this lies in the different shapes at different locations of the SAA and technical differences in the employed instruments. This effect is also observed by Casadio & Arino (priv. comm.) for different altitudes.

The turbulences and the aftermath of the so called Halloween storm 2003 might, at the measured energies, be a reason for the chaos seen in the drift plots. Due to the overlaid structure mentioned before, the fits especially during the period of 2003 until 2006 do not identify the actual maximum. Taking all data points into account with their Poisson statistic errors, the fit often lies above the actual continuum (compare figure 2.5 on page 19). As can easily be seen, trying to shift the fit to the continuum, and therefore willingly accepting worse  $\chi^2$  values, varies the maximum of the fit for about  $\pm 2^\circ$ . In some cases, like for example the Gumbel fit for protons in 2003.75 where the best fit shifts the maximum between the real maximum and a really prominent side lobe, the impact is even worse. Hence, the derived longitude values are not quite reliable in the noisy time interval. That makes a serious interpretation of changes in the movement of the SAA quite unrealistic.

Nevertheless, similar structures in between the unreliable data, which are reproduced in all of the four approaches to maximum determination, imply that the 2003 change in direction of the movement seen by Fürst et al. (2009) and confirmed by Casadio & Arino (priv. comm.) is also measured by *RHESSI*. Unfortunately, the dispersion of the derived maximum positions does not allow for a broken line fit to sufficiently find the time of the slope change. Therefore, only a linear fit over the whole data sample is done, which leads to an average slope of  $0.605 \pm 0.021^\circ \text{ yr}^{-1}$ . This value rises slightly above the predicted drift rate of  $0.3^\circ \text{ yr}^{-1}$  to  $0.5^\circ \text{ yr}^{-1}$  from former investigations. But this average includes only a relatively small time period compared to former attempts that have compared data taken decades apart. As already indicated by Fürst (2008) the drift rate of  $\sim 0.3^\circ \text{ yr}^{-1}$  seems to be only valid for longer time scales and underlies supplementary variations. Table 2.2 on page 26 lists the fitted slopes for the different latitudes and particles. The Weibull fits alone agree far better with the Fürst (2008) results at the same latitude while the more southern applied Gumbel fits seem to cause the excess in the drift rate. Moreover, in total the proton SAA drift rate tends to be greater than the drift rate of the electron SAA in both latitudes. This effect might be ascribed to the fact that the SAA drift and the drift of positively charged particles in the magnetic field head into the same direction, namely westwards.

As a simple straight line is not able to account for the complexity of the drift but also the statistic is too bad for a more detailed function, as a compromise additionally a linear fit over the time period of 2006.25 until 2010.25 on its own is applied, where the obtained parameters of the Weibull respectively Gumbel fits are less biased (see figure 2.6 on page 20). Figure 2.13 on page 26 clearly shows that the accordance between data and fit function is far better, especially for the protons, which throughout the whole analysis appear less noisy due to their higher energy, whereas the consensus of the resulting slopes (table 2.3 on page 26) with previous results is even worse. Besides, the relative strengths of the drift between the electrons and protons and the center and the edge of the SAA respectively are reversed with respect to the results of the fit over the complete time span.

Fürst et al. (2009) linked the breaks in the drift direction of the SAA maximum with geomagnetic jerks. A geomagnetic jerk is a jump in the second derivative of the magnetic field strength and occurs due to a jump in the acceleration in the fluid motion at the core-mantle-boundary (Olsen & Manda, 2007a). As the SAA is linked to the geomagnetic field, it is only reasonable to suspect changes in the magnetic field having an influence on the evolution of the SAA. Although not worldwide in occurrence (Olsen & Manda, 2007a), Olsen & Manda (2007b) state that the 2003 jerk, which was centered between Eastern Asia and Australia, probably even had an impact on the drift of the north magnetic dip pole, hence having an exceptional influence on the geomagnetic field. Furthermore, Fürst et al. (2009) matched a break of the SAA drift in the

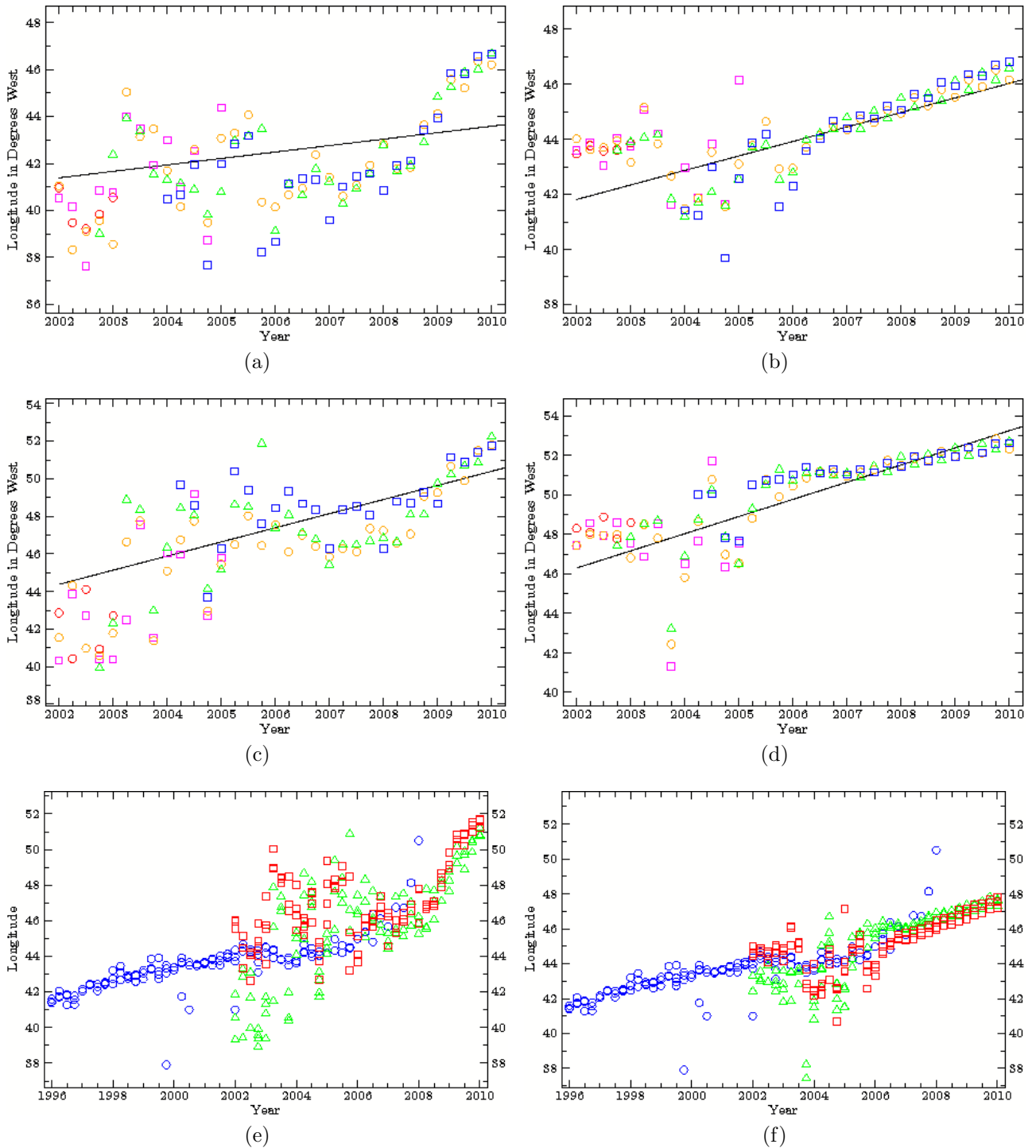


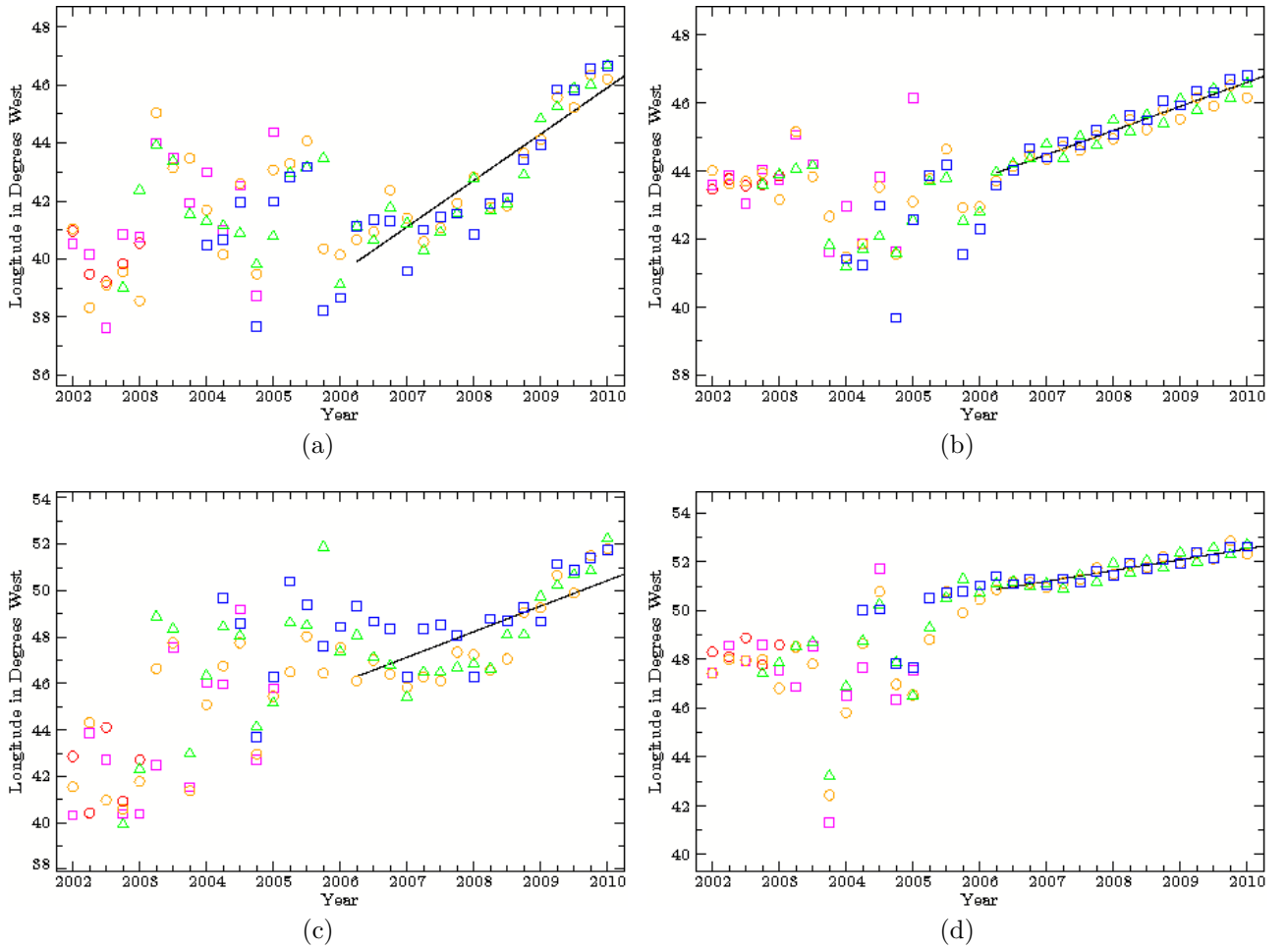
**Figure 2.12:** Position of maximum: (a) electrons and (b) protons at latitude  $-23^\circ$  and (c) electrons and (d) protons at latitude  $-31^\circ$  south; colors represent the altitude as listed in 2.1. (e) (electrons) and (f) (protons) show the fitted positions of Weibull (red) and Gumbel (green) compared to the RXTE results (blue); the maximum positions of the Weibull fits are shifted  $5^\circ$  (electrons) resp.  $1^\circ$  (protons) westwards whereas those of the Gumbel fits are shifted  $1^\circ$  (electrons) resp.  $5^\circ$  (protons) eastwards to match the RXTE results.

**Table 2.2:** *The slope for the straight line fits over the complete available time periods.*

Latitude	Fitting function	Electrons	Protons
$-23^\circ$	Weibull	$0.274 \pm 0.016$	$0.527 \pm 0.014$
$-31^\circ$	Gumbel	$0.752 \pm 0.001$	$0.869 \pm 0.002$

**Table 2.3:** *The slope for the straight line fits over the time interval 2006.25–2010.0.*

Latitude	Fitting function	Electrons	Protons
$-23^\circ$	Weibull	$1.599 \pm 0.035$	$0.708 \pm 0.048$
$-31^\circ$	Gumbel	$1.102 \pm 0.004$	$0.442 \pm 0.005$

**Figure 2.13:** *Position of maximum with a linear fit from 2006.25 on: (a) electrons and (b) protons at latitude  $-23^\circ$  and (c) electrons and (d) protons at latitude  $-31^\circ$  south; colors represent the altitude as listed in 2.1.*

first half of 1998 with a geomagnetic jerk that occurred around 1999. Casadio & Arino (priv. comm.) agree with an drift anomaly around 2003. They date this anomaly to the 2002-2003 interval while Fürst et al. (2009) see the beginning rather in early 2003 with consequences up to 2004. Besides, Casadio & Arino claim to detect the 1991 jerk within a fast reversal drift speed of the SAA but at the same time these data points are excluded from their plots with the justification that this year is not completely covered by the missions employed for their analysis. In contrast, in the same data set there is an event obvious during the 1995-1996 period. For this time no evidence for a geomagnetic jerk can be found in the literature. Actually, Casadio & Arino explain this discrepancy by their data being more noisy during that time than at other times.

There is evidence for a further jerk of presumably non-global extent between 2006 and 2008 located at South Africa and the South Atlantic Ocean, though measured at slightly different times at different locations (Chulliat et al., 2010). In the following this jerk will be referred to as the 2007 jerk. But as the maximum positions derived by *RHESSI* data are quite discordant in the period of 2003 to 2006, it is not possible to give a reliable statement whether the slight knee that can be seen in the longitude plots for the electrons and is almost not visible for the protons (figure 2.13 on the facing page) is an effect of the satellite or if there is any evidence for the same break in the SAA drift rates obtained by *RHESSI* data. Unfortunately, just at that time the *RXTE* analysis reaches the end of its data set and, again, the jerk is not referred to by Casadio & Arino. Therefore, this most recent jerk can not yet be used to resolve the question whether or not geomagnetic jerks can be accused to cause those abrupt changes in the movement of the SAA.

Even so the question is left open what causes different geomagnetic jerks to be so differently severe in their impact on the SAA evolution. Why is the effect of the 2003 jerk so prominent while the 2007 jerk which was located closer at the region of the SAA and one of the strongest jerks of the last century (Chulliat et al., 2010) is nearly not even recognized? Maybe geomagnetic jerks have to possess certain properties to increase their influence. Or there has to be a coincidence between two or more. According to Baker et al. (2004) there have been two impetuous solar storms violently distorting the radiation belts and injecting huge amounts of energetic charged particles into the atmosphere that nearly happened during the same time as the geomagnetic jerks in 1991 and 2003. Between these two years there have not occurred any solar storms of comparable strength. If Casadio & Arino are right with their pronouncement to actually see the 1991 jerk in a significant change of drift of the SAA maximum, it could be the combination of the jerks with the solar storms, which again caused geomagnetic storms, that resulted in these extraordinary strong aberration of the SAA drift direction.

# Chapter 3

## Outlook

There are still plenty of findings hidden behind the *RHESSI* data. The origin of the quasi-periodical substructure overlaid on the continuum of the radiation background has to be determined. Either it can be filtered by approaches like the boxcar method or by averaging over longer time periods to mark all measurements that differ by more than three standard deviations from the mean value and then return to finer resolution again, or it might turn out to be a so far unregarded phenomenon that is worth to be studied. In the latter case also a way should be looked for to efficiently smooth the data to obtain better statistics for the rest of the examination. Maybe some of the more prominent peaks of the substructure should be treated as emission lines by adding additional functions such as Gaussian distributions to the fit to maintain more accurate models of the continuum. An examination of the positioning algorithm of *RHESSI* and the performance of the particle detectors also might lead to insights into the formation of the substructure. Then the possibility of applying a two dimensional fit of the SAA maximum should be respected, thus the drift of the maximum position in latitudinal direction can also be analyzed. Badhwar (1997) for example argue that the latitude drift rate is not resolvable by only using the peak of the particle distribution. It would be interesting to verify or disapprove that with the higher resolution of *RHESSI*. Moreover, geomagnetic jerks as trigger for sudden directional changes of the SAA movement have to be explored further. Possibly, certain circumstances like geomagnetic jerks, coronal mass ejections and geomagnetic storms have to coincide to cause those changes in the SAA drift rate as observed. An extension of the *RXTE* analysis to the data up to 2010 will probably help to sort this issue out. At any rate, there is still much to be found out about the evolution of the South Atlantic Anomaly and the possible causes for its change with time.

# Bibliography

- Adolphsen J., Barth J.L., Stassinopoulos E.G., et al., 1995, IEEE Trans. Nuc. Sci. 42, 1964
- Antal T., Sylos Labini F., Vasilyev N.L., Baryshev Y.V., 2009, Europhysics Letters 88, 59001
- Badavi F.F., Nealy J.E., deAngelis G., et al., 2005, In: Space 2005., AIAA, p.1
- Badhwar G.D., 1997, J. Geophys. Res. 102, 2343
- Badhwar G.D., Konradi A., Braby L.A., et al., 1994, Adv. Space Res. 14, 67
- Baker D.N., Kanekal S.G., Li X., et al., 2004, Nature 432, 878
- Barlow J., 1989, Statistics: A guide to the use of statistical methods in the physical sciences, John Wiley and Sons
- Barth J.L., Dyer C.S., Stassinopoulos E.G., 2003, IEEE Trans. Nuc. Sci. 50, 466
- Bühler P., Desorgher L., Yehnder A., et al., 1996, Radiat. Meas. 26, 917
- Chulliat A., Thebault E., Hulot G., 2010, Geophysical Research Letters 37, 7301
- Dachev P., Tomov B.T., Matviichuk Y.N., et al., 1999, Rad. Meas. 30, 269
- Elsasser W.M., 1946, Phys. Rev. 69, 106
- Fraser-Smith A.C., 1987, Reviews of Geophysics 25, 1
- Fürst F., 2008, Investigations of the SAA and the long-time behavior of Vela X-1
- Fürst F., Wilms J., Rothschild R.E., et al., 2009, EPSL 281, 125
- Gaffey, Jr. J.D., Bilitza D., (eds.) 1990, The NSSDC trapped radiation model facility
- Garrett H.B., Hastings D., 1994, In: 32nd Aerospace Sciences Meeting & Exhibit., AIAA, Reston, p.590
- Ginet G.P., Madden D., Dichter B.K., Brautigam D.H., 2007, In: Radiation Effects Data Workshop., IEEE
- Grigoryan O.R., Petrov A.N., Romashova V.V., 2005, In: WDS '05 Proceedings of Contributed Papers, Vol. 2., Matfyzpress, Prague, p.251
- Grigoryan O.R., Romashova V.V., Petrov A.N., 2008, Adv. Space Res. 41, 76
- Hajdas W., Eggel C., Wigger C., et al., 2004, In: Fletcher K. (ed.) Proc. Radiation and its Effects on Components and Systems, RADECS 2003. ESA SP-536, Noordwijk, p.607
- Heirtzler J., 2002, Journal of Atmospheric and Solar-Terrestrial Physics 64, 1701

- Heynderickx D., 1996, *Rad. Meas.* 26, 369
- Huston S.L., Kuck G.A., Pfitzer K.A., 1996, In: Lemaire J.F., Heyndericks D., Baker D.N. (eds.) *Radiation Belts: Models and Standards.*, AGU, Washington, p.119
- Konradi A., Badhwar G.D., Braby L.A., 1994, *ASR* 14, 911
- Lauriente M., Vampola V.L., Gosier K., 1996, In: Lemaire J.F., Heyndericks D., Baker D.N. (eds.) *Radiation Belts: Models and Standards.*, AGU, p.109
- Li X., Baker D.N., Temerin M., et al., 1997, *Geophysical Research Letters* 24, 923
- McIlwain C.E., 1966, *Space Science Reviews* 5, 586
- Mullen E.G., Ginet G., Gussenhoven M.S., Madden D., 1998, *IEEE Trans. Nuc. Sci.* 45, 2954
- Olsen N., Manda M., 2007a, *Earth Planet. Sci. Lett.* 255, 94
- Olsen N., Manda M., 2007b, *EOS Transactions* 88, 293
- Pinto, Jr. O., Gonzalez W.D., Pinto I.R.C.A., et al., 1992, *J. Atmos. Terrest. Phys.* 54, 1129
- Prölss G.W., 2001, *Physik des erdnahen Weltraums : Eine Einführung*, Springer-Verlag Berlin Heidelberg New York
- Roberts P.H., Glatzmaier G.A., 2000, *Rev. Modern Phys.* 72, 1081
- Sawyer D.M., Vette J.I., 1976, *NASA STI/Recon Technical Report N 77*, 18983
- Smith D.M., Lin R.P., Turin P., et al., 2002, *Solar Physics* 210, 33
- Vette J.I., 1991, *NASA STI/Recon Technical Report N 92*, 24228

# Acknowledgements

First I want to thank Jörn Wilms, the supervisor of my Bachelor thesis, for providing me with such a fascinating issue. Although his major research interest is in black holes and neutron stars, he always keeps an open mind for other exciting topics.

My further gratitude belongs to Felix Fürst with whom I worked together on this project. He introduced me to the programs used for the analysis and greatly supported me all the time. I really appreciate the inspiring discussions we had about the SAA and other topics. This work is based on and continues his examination of the South Atlantic Anomaly using *RXTE* data. In addition, I'd like to thank the X-ray astronomy work group of the Dr. Karl Remeis observatory for the fantastic ambience in the office. They took care of quite the right amount of distraction during and after work. At the same time they have always been available for competent council. Namely, Manfred Hanke, Moritz Böck and Thomas Dauser, who never got tired of answering questions about isis and pointed out many nice functions to me.

A special thanks goes to my friends and family who patiently listened to me both when exciting results arised and when everything seemed to be confusing.



# Erklärung

Hiermit bestätige ich, dass ich diese Arbeit selbstständig und nur unter Verwendung der angegebenen Hilfsmittel angefertigt habe.

Erlangen,

Natalie Hell